LETTER

doi:10.1038/nature13235

Emergence of reproducible spatiotemporal activity during motor learning

Andrew J. Peters[1], Simon X. Chen[1] & Takaki Komiyama[1,2]

The motor cortex is capable of reliably driving complex movements[1,2] yet exhibits considerable plasticity during motor learning[3–10]. These observations suggest that the fundamental relationship between motor cortex activity and movement may not be fixed but is instead shaped by learning; however, to what extent and how motor learning shapes this relationship are not fully understood. Here we addressed this issue by using *in vivo* two-photon calcium imaging[11] to monitor the activity of the same population of hundreds of layer 2/3 neurons while mice learned a forelimb lever-press task over two weeks. Excitatory and inhibitory neurons were identified by transgenic labelling[12,13]. Inhibitory neuron activity was relatively stable and balanced local excitatory neuron activity on a movement-by-movement basis, whereas excitatory neuron activity showed higher dynamism during the initial phase of learning. The dynamics of excitatory neurons during the initial phase involved the expansion of the movement-related population which explored various activity patterns even during similar movements. This was followed by a refinement into a smaller population exhibiting reproducible spatiotemporal sequences of activity. This pattern of activity associated with the learned movement was unique to expert animals and not observed during similar movements made during the naive phase, and the relationship between neuronal activity and individual movements became more consistent with learning. These changes in population activity coincided with a transient increase in dendritic spine turnover in these neurons. Our results indicate that a novel and reproducible activity–movement relationship develops as a result of motor learning, and we speculate that synaptic plasticity within the motor cortex underlies the emergence of reproducible spatiotemporal activity patterns for learned movements. These results underscore the profound influence of learning on the way that the cortex produces movements.

We developed a cued lever-press task performed by mice under a two-photon microscope (Fig. 1a), similar to other recently reported tasks[14,15]. Briefly, a lever press beyond the set threshold during an auditory cue was rewarded with water (Methods). Mice were trained with this task daily for 2 weeks ($n = 10$). Even though mice achieved a reward in most trials, the timing of their behaviour improved in later sessions (Extended Data Fig. 1). Furthermore, lever movements on individual trials became more stereotyped over time (Fig. 1b). The reproducibility of movement

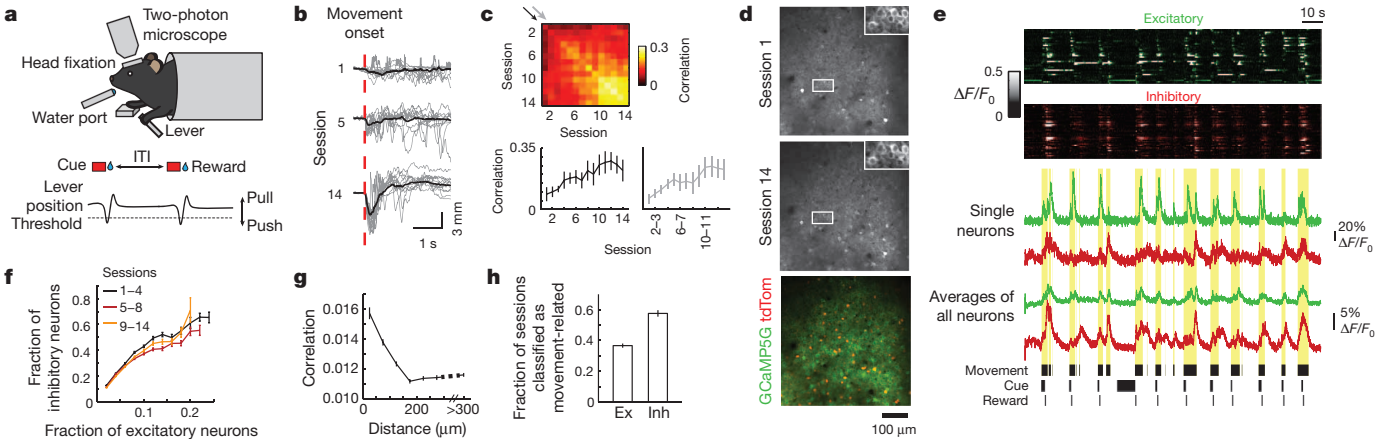

Figure 1 | Lever-press task and chronic calcium imaging of excitatory and inhibitory populations. **a**, Task schematic. **b**, Lever movement traces in rewarded trials from one mouse. Grey, 10 individual trials; black, average of all trials; red dotted line, movement onset. **c**, Top: median pairwise correlation coefficients of rewarded movements on individual trials over 3 s, averaged across animals. Bottom: pairwise movement correlation on individual trials within and across sessions corresponding to the black and grey arrows indicated on the top, respectively. Individual movements became more similar within ($r = 0.35$, $P < 0.001$) and across ($r = 0.37$, $P < 0.001$) sessions. See Methods for sample size. **d**, Top and middle: GCaMP5G expression in layer 2/3 neurons imaged 2 weeks apart. Insets: magnified images of outlined areas. Bottom: merge of tdTomato expressed in all inhibitory neurons (red) and GCaMP5G (green). **e**, Top: activity of all simultaneously imaged movement-related 38 excitatory (green) and 42 inhibitory (red) neurons from one animal. Each row represents a neuron. Middle: $\Delta F/F_0$ traces from one neuron each and average $\Delta F/F_0$ of all imaged neurons of each type (152 excitatory and 77 inhibitory). Bottom: task-related events; yellow shading indicates movement epochs. **f**, Fractions of active inhibitory neurons and excitatory neurons during rewarded movements are correlated on a movement-by-movement basis ($r = 0.63$–0.67, $P < 0.001$). This relationship is stable throughout learning ($P = 0.92$, one-way ANOVA comparison of median excitatory/inhibitory ratios). **g**, Pairwise correlation coefficients between inhibitory and excitatory neuron activity decrease with distance ($P < 0.001$, comparison between pairs within 150 μm and all other pairs, Wilcoxon rank sum test, $n = 653{,}046$ excitatory–inhibitory pairs total). **h**, Individual movement-related inhibitory neurons are classified on more sessions, showing that excitatory neurons are on average more dynamic than inhibitory neurons ($P < 0.001$, Wilcoxon rank sum test, $n = 473$ and 231 movement-related excitatory and inhibitory neurons, respectively). All error bars are s.e.m.

[1]Neurobiology Section, Center for Neural Circuits and Behavior, and Department of Neurosciences, University of California, San Diego, La Jolla, California 92093, USA. [2]JST, PRESTO, University of California, San Diego, La Jolla, California 92093, USA.

©2014 Macmillan Publishers Limited. All rights reserved

kinematics was evident in higher correlation of rewarded movements on individual trials within and across later sessions (Fig. 1c). The motor cortex is necessary for this task, as lesions before training prevented the emergence of movement stereotypy, and acute inactivation by pharmacology or optogenetics impaired task performance (Extended Data Fig. 2).

To identify how the activity of motor cortex neuronal ensembles is modified during this learning, we combined the lever-press task with chronic two-photon calcium imaging[8,16]. In this study we focused on neurons in layer 2/3, the major input layer capable of driving deeper layer neurons to produce motor cortex outputs[17,18]. Before training, we injected an adeno-associated virus encoding the Ca^{2+} indicator GCaMP5G[19] into the right forelimb area of the motor cortex to express GCaMP5G in all neuron types. Optogenetic stimulation of this area evoked forelimb movements (Extended Data Fig. 3). GCaMP5G fluorescence reported spiking activity with high temporal precision (jitter of spikes and calcium events = 7.1 ± 41.4 ms, median ± standard deviation (s.d.); Extended Data Fig. 4). We used transgenic mice that express tdTomato in all GABAergic inhibitory neurons (*Gad2-IRES-Cre* (ref. 12); *Rosa-LSL-tdTomato* (ref. 13)) to identify excitatory (only expressing GCaMP5G) and inhibitory (expressing both tdTomato and GCaMP5G) neurons. Two weeks after surgery, hundreds of neurons were imaged through a chronic window. A total of 202 ± 18 (mean ± standard error of the mean (s.e.m.)) neurons were imaged in each animal, with 20.9 ± 2.6% being inhibitory, consistent with the composition of the cortex[20].

We imaged the activity of the same population of excitatory and inhibitory neurons over the course of 2 weeks while mice simultaneously learned and performed the lever-press task (Fig. 1d, $n = 7$ mice). High correlations of neural activity and lever-press movements were evident both at the level of single neurons and population average in both excitatory and inhibitory neurons (Fig. 1e). A large fraction of imaged neurons showed significantly more activity during lever-press movements and were thus considered movement-related (51.4 ± 5.7% of imaged neurons, 44.0 ± 6.2% of excitatory and 78.7 ± 5.7% of inhibitory, were classified as movement-related in at least one session; Methods). Movement-related neurons did not show obvious spatial clustering (Extended Data Fig. 5).

We investigated the relationship between excitatory and inhibitory populations. We found a positive correlation between the fraction of active inhibitory and excitatory neurons on a movement-by-movement basis; during movements that activated a larger fraction of excitatory neurons, a larger fraction of inhibitory neurons were also active. This relationship of excitatory and inhibitory activity remained constant for the entire 2 weeks of imaging (Fig. 1f). Individual inhibitory neurons were particularly correlated with nearby excitatory neurons within 150 μm, consistent with their connectivity[21,22] (Fig. 1g). This local matching of excitatory and inhibitory activity probably provides a basis for the balance between excitatory and inhibitory inputs to individual neurons observed in the cortex (reviewed in ref. 20). Even though the ratio of excitatory and inhibitory

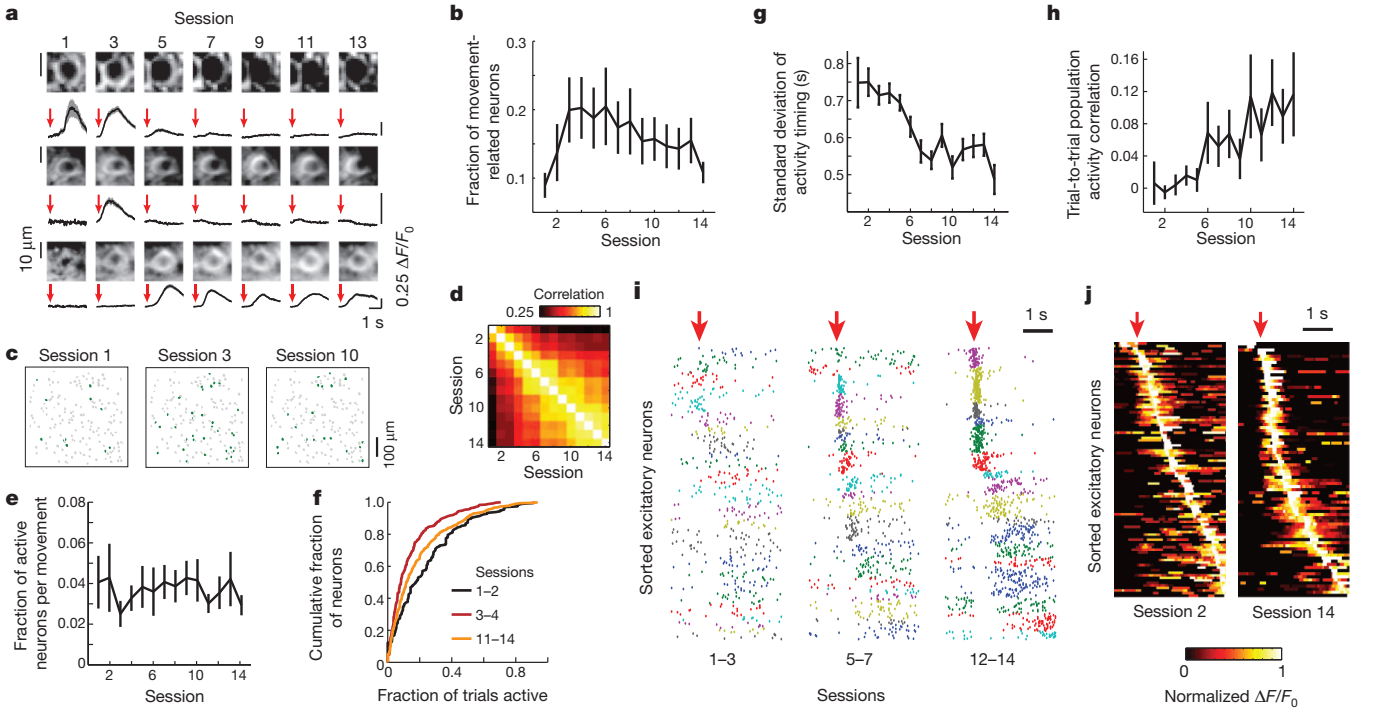

Figure 2 | Dynamics of spatiotemporal activity of excitatory neurons during learning. **a**, Dynamics of three excitatory neurons. Top rows: images of neurons confirming reliable identification. Bottom rows: black, mean $\Delta F/F_0$; grey, s.e.m.; arrow, movement onset. **b**, Mean fraction of excitatory neurons classified as movement-related in each session (increase over sessions 1–3, $P < 0.01$; decrease over sessions 4–14, $P < 0.01$, Methods). **c**, Dynamic population of excitatory neurons from one mouse. Green, movement-related excitatory neurons; grey, non-classified excitatory neurons. **d**, Correlation of population activity of all excitatory neurons during rewarded movements across sessions (Methods). The population of movement-related excitatory neurons became more stable in later sessions ($P < 0.001$, session 1–4 pairs versus session 10–14 pairs, Wilcoxon rank sum test). **e**, Average fraction of excitatory neurons that are active in each individual movement out of all excitatory neurons remains stable throughout learning ($r = 0.00$, $P = 0.98$). **f**, Cumulative distribution of fraction of trials in which each movement-related excitatory neuron is active. In sessions 3–4, individual movement-related neurons are active in fewer trials compared to sessions 1–2 or 11–14 ($P < 0.001$, Kolmogorov–Smirnov test). **g**, Standard deviation of the timing of activity onsets for movement-related excitatory neurons decreases over sessions ($r = -0.24$, $P < 0.001$). Neurons that were active in less than five trials of a given session were excluded from this analysis. **h**, Pairwise trial-to-trial correlation of temporal population activity vectors increases with learning ($r = 0.43$, $P < 0.001$). Temporal population activity vector was a concatenation of the activity traces of all movement-related neurons and thus maintained temporal information within each movement. **i**, Activity onsets of excitatory neurons from one animal that are movement-related and active in at least 10% of trials on the sessions indicated. Arrow, movement onsets; colours, individual neurons sorted according to their preferred timing. Note that same colours across sessions are not necessarily the same neurons. **j**, Maximum-normalized average activity from all movement-related neurons from all animals in session 2 (left, 106 neurons) and session 14 (right, 84 neurons) aligned to movement onset (arrow). Activity timing is refined over time, shown by narrower peaks and lower background in session 14, and shifts towards movement onset. See Methods for sample size. All error bars are s.e.m.

©2014 Macmillan Publishers Limited. All rights reserved

activity on a trial-to-trial basis was stable, the identity of movement-related neurons was dynamic. In particular, excitatory neurons on average had a higher degree of turnover than the inhibitory population, indicating that the excitatory population is more dynamic during learning (Fig. 1h and Extended Data Fig. 6a). We therefore focused on excitatory neurons for the following analyses.

Many excitatory neurons were transiently movement-related (Fig. 2a). In the initial phase of learning, a large fraction of excitatory neurons developed movement-related activity, resulting in a marked increase of the movement-related population (Fig. 2b, c). After this initial expansion, the fraction of movement-related neurons decreased gradually through the remaining course of the experiment (Fig. 2b, c and Extended Data Fig. 6b). This resulted in a smaller and more stable population of movement-related neurons towards the end of learning (Fig. 2d). The expansion and refinement was not seen during spontaneous movements without training (Extended Data Fig. 6c). Despite these changes in the ensemble of movement-related neurons during learning, the average fraction of excitatory neurons active on each trial remained stable (Fig. 2e). This constant level of activity was maintained despite a changing size of movement-related populations because of the corresponding shift in the frequency of activity in individual neurons (Fig. 2f). Various combinations of excitatory neurons were therefore used within the motor cortex during the initial phase of learning, followed by a refinement of the population to form a stable network associated with the learned movement.

We next examined the timing of activity of individual neurons. As a population, the activity of movement-related excitatory neurons diverged from baseline at 105 ms before the movement onset and continued throughout the duration of movements (Extended Data Fig. 6d). During the first few sessions of learning, movement-related excitatory neurons showed variable timing of activity on individual trials relative to the movement onset. Conversely, movement-related neurons in later sessions showed reproducible activity timing relative to movement onset (Fig. 2g and Extended Data Fig. 6e). As a result, the temporal activity pattern became progressively more stable during learning (Fig. 2h). This activity sequence tiled the entire duration of movement (Fig. 2i, j and Extended Data Fig. 6f). Furthermore, the population activity shifted towards the beginning of movements over the course of the experiment (Fig. 2j and Extended Data Fig. 6g).

The observed stabilization of motor cortex activity may result from the selection of a particular activity–movement pair out of many that are explored during initial learning. In this case, activity during the learned movement and activity during similar movements made early in learning should resemble each other. Alternatively, the 'learned' activity pattern may be unique to the expert stage after learning. To distinguish between these possibilities, we evaluated the relationship between movement and neural activity. We defined the 'learned' patterns of activity and movement as the averages of a randomly chosen 50% of trials from the expert sessions (sessions 10–14, Methods). When the remaining 50% of trials from the expert sessions were sorted according to the similarity of the movement in each trial with the learned movement pattern, a clear relationship between movement and activity became evident—the similarity of activity to the learned activity pattern increased with the similarity of movements to the learned movement (Fig. 3a, b). Remarkably, this relationship was much weaker when trials from naive sessions (sessions 1–3) were considered. Regardless of the similarity of movement to the learned movement pattern, the similarity of activity to the learned activity pattern was consistently low in naive sessions (Fig. 3a, b). In other words, the learned activity pattern was reproducibly observed only when the expert animals made the learned movement, whereas similar movements made in naive sessions were accompanied by very different activity patterns. Furthermore, the general relationship between activity and movement in pairs of trials became more consistent after learning, whereas activity in naive animals was more variable regardless of movement similarity (Fig. 3c). These analyses of learning-related changes in population activity were performed using the entire movement periods. However,

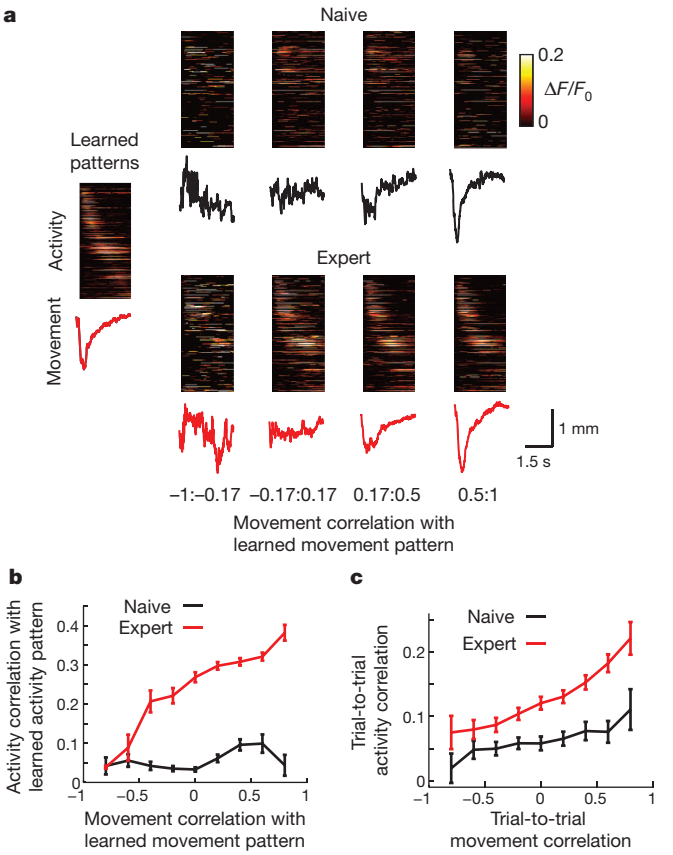

Figure 3 | Learning-related emergence of reproducible spatiotemporal activity. **a**, Heat maps show mean activity of movement-related excitatory neurons classified during expert sessions of all animals aligned to movement onset (left edge). Traces show mean lever movements. Trials are binned according to the correlations of the movements on those trials with the learned movement pattern (Methods). Left, learned patterns; top, naive sessions (sessions 1–3); bottom, expert sessions (sessions 10–14). **b**, Correlation of trial activity with the learned activity pattern increases with the correlation of trial movement with the learned movement pattern in expert sessions. Movements similar to the learned movement pattern but made in naive sessions display activity very different from the learned activity pattern ($P = 0.83$, 0.35 and <0.001 in the bins 1, 2 and 3–9, respectively, Wilcoxon rank sum test). **c**, Pairwise trial-to-trial correlation of temporal population activity vectors (defined as in Fig. 2h) plotted as a function of movement correlation on those trials. A stronger relationship between population activity and movement emerges during learning ($P = 0.38$, 0.18, 0.04, 0.002, <0.001 and 0.02 in bins 1, 2, 3, 4, 5–8 and 9, respectively, Wilcoxon rank sum test). See Methods for sample size. All error bars are s.e.m.

the results were similar when only the periods from movement onset to reward were considered (Extended Data Fig. 7).

The plasticity of population activity described above could simply reflect changes in other brain areas providing inputs to these neurons. However, synaptic plasticity within the motor cortex could also contribute to the changes in population activity. To test whether learning of this lever-press task induces synaptic plasticity in layer 2/3 of the motor cortex, we labelled sparse subsets of layer 2/3 neurons and chronically imaged spines on the same dendritic branches of excitatory neurons over the course of learning ($n = 191$ spines in 3 mice). Imaging was performed immediately before each training session in awake animals. We observed the formation of a number of dendritic spines during the initial sessions of training, followed by the elimination of some of the spines that were present at the beginning of the experiment. Most (95%, 19 out of 20) of the spines that formed during training persisted for the entire 2 weeks. At the population level, these changes resulted in a transient 10% increase in the density of spines followed by return to the baseline

©2014 Macmillan Publishers Limited. All rights reserved

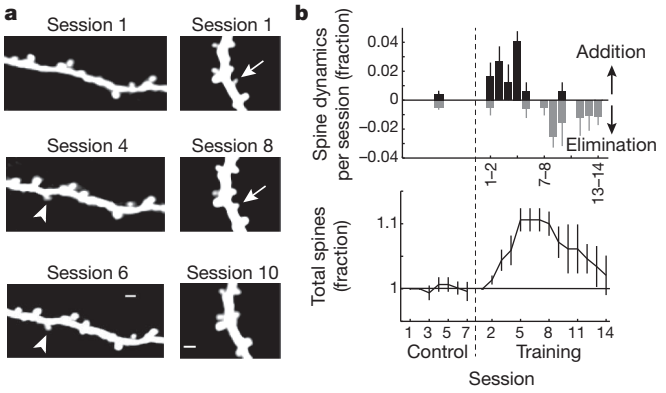

Figure 4 | Learning-related plasticity of dendritic spines. a, Example layer 2/3 excitatory neuron dendrites imaged in awake mice throughout learning. Arrowheads, added spine; arrows, eliminated spine; scale bars, 2 μm. **b**, Summary of spine dynamics in trained and control animals. Top: spine additions (black) and eliminations (grey) in each session. For control animals, data from all sessions are combined. Bottom: total spine number across sessions normalized to session 1 in each condition. Spine density transiently increases during learning ($P < 0.001$, control versus training sessions 4–7, Wilcoxon rank sum test). $n = 191$ spines in 3 mice. All error bars are s.e.m.

(Fig. 4). These results are analogous to previous reports in motor cortex layer 5 neurons during different motor learning tasks[3,4]. Spines were largely stable in a separate group of animals that did not undergo training but otherwise were treated identically including water restriction and head fixation (Fig. 4b). The spine density was also stable in the hindlimb area in the motor cortex during learning (Extended Data Fig. 8). These results indicate that our lever-press task induces area-specific reorganizations of excitatory synapses onto layer 2/3 neurons during learning.

Previous studies suggested a relatively stable tuning and population code of motor cortex neurons in well-trained animals[23,24]. However, our understanding is quite limited as to the changes in the ensemble activity pattern during the transition from naive to expert stages. Our results indicate that the relationship between movements and activity is initially inconsistent (that is, degenerate), and the early days of learning involve the expansion and exploration of various movement-related activity in the motor cortex. An increased variability of single-neuron activity in the motor cortex has been observed during learning of visuomotor adaptation[25] and a brain–machine interface task[26]. Such trial-to-trial variability has been proposed to provide the basis for exploration of possible network states and facilitate learning[10]. Our results directly demonstrate such an exploration during initial learning at the population level. After this period of high variability, the activity–movement degeneracy is reduced and a reproducible temporal sequence of activity emerges in a stable population of excitatory neurons (Extended Data Fig. 9). Such spatiotemporal activity may orchestrate the temporal dynamics of the learned movement. Reproducible temporal patterns of population activity during learned movements are proposed to be generated by internal connections within the motor cortex[27,28]. We note that our results do not provide a causal link between local synaptic plasticity and changes in population activity. Nevertheless, we show that these processes occur during motor learning on similar timescales, which supports the notion that local synaptic plasticity may generate a circuit to reproduce a particular spatiotemporal activity pattern. These new circuits may be more efficient in driving movements, which could underlie the lower metabolic activity in the motor cortex observed during execution of well-practiced movements[29,30]. Our study provides a glimpse of the emergence of population activity patterns for learned movements.

METHODS SUMMARY

Surgeries were performed to inject viruses in the right forelimb area of the motor cortex and implant a chronic window and head plate. For functional imaging, AAV2/1-Syn-GCaMP5G was injected in *Gad2-IRES-Cre; Rosa-LSL-tdTomato* mice; for structural imaging, a mixture of AAV2/1-CAG-FLEX-EGFP and AAV2/1-CMV-PI-Cre was injected in C57BL/6 mice. Imaging and behaviour experiments started at least 2 weeks after surgery and mice were at least 8 weeks of age. Imaging was performed in awake mice during (functional imaging) or right before (structural imaging) each behavioural session.

Online Content Any additional Methods, Extended Data display items and Source Data are available in the online version of the paper; references unique to these sections appear only in the online paper.

Received 9 August 2013; accepted 7 March 2014.
Published online 4 May 2014.

1. Graziano, M. S. A. *The Intelligent Movement Machine* 1st edn (Oxford, 2009).
2. Harrison, T. C., Ayling, O. G. & Murphy, T. H. Distinct cortical circuit mechanisms for complex forelimb movement and motor map topography. *Neuron* **74,** 397–409 (2012).
3. Xu, T. *et al.* Rapid formation and selective stabilization of synapses for enduring motor memories. *Nature* **462,** 915–919 (2009).
4. Yang, G., Pan, F. & Gan, W. B. Stably maintained dendritic spines are associated with lifelong memories. *Nature* **462,** 920–924 (2009).
5. Nudo, R. J., Milliken, G. W., Jenkins, W. M. & Merzenich, M. M. Use-dependent alterations of movement representations in primary motor cortex of adult squirrel monkeys. *J. Neurosci.* **16,** 785–807 (1996).
6. Rioult-Pedotti, M. S., Friedman, D. & Donoghue, J. P. Learning-induced LTP in neocortex. *Science* **290,** 533–536 (2000).
7. Komiyama, T. *et al.* Learning-related fine-scale specificity imaged in motor cortex circuits of behaving mice. *Nature* **464,** 1182–1186 (2010).
8. Huber, D. *et al.* Multiple dynamic representations in the motor cortex during sensorimotor learning. *Nature* **484,** 473–478 (2012).
9. Sanes, J. N. & Donoghue, J. P. Plasticity and primary motor cortex. *Annu. Rev. Neurosci.* **23,** 393–415 (2000).
10. Rokni, U., Richardson, A. G., Bizzi, E. & Seung, H. S. Motor learning with unstable neural representations. *Neuron* **54,** 653–666 (2007).
11. Stosiek, C., Garaschuk, O., Holthoff, K. & Konnerth, A. *In vivo* two-photon calcium imaging of neuronal networks. *Proc. Natl Acad. Sci. USA* **100,** 7319–7324 (2003).
12. Taniguchi, H. *et al.* A resource of Cre driver lines for genetic targeting of GABAergic neurons in cerebral cortex. *Neuron* **71,** 995–1013 (2011).
13. Madisen, L. *et al.* A robust and high-throughput Cre reporting and characterization system for the whole mouse brain. *Nature Neurosci.* **13,** 133–140 (2010).
14. Isomura, Y., Harukuni, R., Takekawa, T., Aizawa, H. & Fukai, T. Microcircuitry coordination of cortical motor information in self-initiation of voluntary movements. *Nature Neurosci.* **12,** 1586–1593 (2009).
15. Hira, R. *et al.* Spatiotemporal dynamics of functional clusters of neurons in the mouse motor cortex during a voluntary movement. *J. Neurosci.* **33,** 1377–1390 (2013).
16. Kato, H. K., Chu, M. W., Isaacson, J. S. & Komiyama, T. Dynamic sensory representations in the olfactory bulb: modulation by wakefulness and experience. *Neuron* **76,** 962–975 (2012).
17. Weiler, N., Wood, L., Yu, J., Solla, S. A. & Shepherd, G. M. Top-down laminar organization of the excitatory network in motor cortex. *Nature Neurosci.* **11,** 360–366 (2008).
18. Kaneko, T., Cho, R., Li, Y., Nomura, S. & Mizuno, N. Predominant information transfer from layer III pyramidal neurons to corticospinal neurons. *J. Comp. Neurol.* **423,** 52–65 (2000).
19. Akerboom, J. *et al.* Optimization of a GCaMP calcium indicator for neural activity imaging. *J. Neurosci.* **32,** 13819–13840 (2012).
20. Isaacson, J. S. & Scanziani, M. How inhibition shapes cortical activity. *Neuron* **72,** 231–243 (2011).
21. Kwan, A. C. & Dan, Y. Dissection of cortical microcircuits by single-neuron stimulation *in vivo*. *Curr. Biol.* **22,** 1459–1467 (2012).
22. Kätzel, D., Zemelman, B. V., Buetfering, C., Wolfel, M. & Miesenbock, G. The columnar and laminar organization of inhibitory connections to neocortical excitatory cells. *Nature Neurosci.* **14,** 100–107 (2011).
23. Chestek, C. A. *et al.* Single-neuron stability during repeated reaching in macaque premotor cortex. *J. Neurosci.* **27,** 10742–10750 (2007).
24. Georgopoulos, A. P., Schwartz, A. B. & Kettner, R. E. Neuronal population coding of movement direction. *Science* **233,** 1416–1419 (1986).
25. Mandelblat-Cerf, Y., Paz, R. & Vaadia, E. Trial-to-trial variability of single cells in motor cortices is dynamically modified during visuomotor adaptation. *J. Neurosci.* **29,** 15053–15062 (2009).
26. Arduin, P. J., Fregnac, Y., Shulz, D. E. & Ego-Stengel, V. "Master" neurons induced by operant conditioning in rat motor cortex during a brain-machine interface task. *J. Neurosci.* **33,** 8308–8320 (2013).
27. Shenoy, K. V., Sahani, M. & Churchland, M. M. Cortical control of arm movements: a dynamical systems perspective. *Annu. Rev. Neurosci.* **36,** 337–359 (2013).
28. Long, M. A., Jin, D. Z. & Fee, M. S. Support for a synaptic chain model of neuronal sequence generation. *Nature* **468,** 394–399 (2010).
29. Krings, T. *et al.* Cortical activation patterns during complex motor tasks in piano players and control subjects. A functional magnetic resonance imaging study. *Neurosci. Lett.* **278,** 189–193 (2000).

©2014 Macmillan Publishers Limited. All rights reserved

30. Picard, N., Matsuzaka, Y. & Strick, P. L. Extended practice of a motor skill is associated with reduced metabolic activity in M1. *Nature Neurosci.* **16,** 1340–1347 (2013).

Acknowledgements We thank A. Kim and S. Kalina for technical assistance; L. L. Looger, J. Akerboom, D. S. Kim and the GENIE Project at Janelia Farm for making GCaMP available; E. Kyubwa and J. Keller for help with task development; A. D. Lien and M. Caudill for help with two-photon guided recordings; and M. Long, R. Malinow, G. Murphy, M. Scanziani and members of the Komiyama laboratory for comments and discussions. This work was supported by grants from Japan Science and Technology Agency (PRESTO), Pew Charitable Trusts, Alfred P. Sloan Foundation, David & Lucile Packard Foundation, Human Frontier Science Program and New York Stem Cell Foundation to T.K. A.J.P. is supported by the Neuroplasticity of Aging Training Grant (AG000216). S.X.C. is a Human Frontier Science Program postdoctoral fellow. T.K. is a NYSCF-Robertson Investigator.

Author Contributions A.J.P. and T.K. conceived the project. Dendritic spine imaging and optogenetic silencing experiments were performed by S.X.C. and analysed by S.X.C. and T.K. All other experiments were performed by A.J.P. and analysed by A.J.P. and T.K. A.J.P. and T.K. wrote the manuscript with input from S.X.C.

Author Information Reprints and permissions information is available at www.nature.com/reprints. The authors declare no competing financial interests. Readers are welcome to comment on the online version of the paper. Correspondence and requests for materials should be addressed to T.K. (tkomiyama@ucsd.edu).

©2014 **Macmillan Publishers Limited. All rights reserved**

METHODS

Animals. All procedures were in accordance with protocols approved by the UCSD Institutional Animal Care and Use Committee and guidelines of the National Institute of Health. Mice (calcium imaging: cross between *Gad2-IRES-Cre* (ref. 12) and *Rosa26-CAG-LSL-tdTomato* (ref. 13), Jackson laboratories; structural imaging: C57BL/6, Charles River Laboratory) were group housed in disposable plastic cages with standard bedding in a room with a reversed light cycle (12 h–12 h). After surgery, animals were singly housed. Experiments were performed during the dark period. No randomization was used, but internal controls were included whenever possible.

Surgery. Adult mice (6 weeks or older, male and female) were anaesthetized with isoflurane and injected with dexamethasone (2 mg kg^{-1}) and baytril (10 mg kg^{-1}) intramuscularly to prevent brain swelling and infection. A custom head-plate was glued to the skull and craniotomy (~2 mm diameter) was performed as described[31] over the right caudal forelimb area. Viruses (UPenn Vector Core; calcium imaging: AAV2/1-syn-GCaMP5G diluted 1:1–3 in saline, 5–6 sites; structural imaging: AAV2/1-CAG-FLEX-EGFP (1:1) and AAV2/1-CMV-PI-Cre (1:5,000) diluted in saline, 3 sites) were injected in the caudal forelimb area of the motor cortex around the coordinate of 300 μm anterior and 1,500 μm lateral from bregma, according to previous microstimulation experiments[15,32–36]. We confirmed that optogenetic stimulation of this area evoked forelimb movements (Extended Data Fig. 3). This area also falls near the border of the abduction and adduction areas defined by ref. 2. For control experiments targeting the hindlimb area of the motor cortex, viruses were injected around the coordinate of 1,500 μm posterior and 1,500 μm lateral from bregma, according to previous microstimulation experiments[32,33,35,36]. Each injection consisted of ~20 nl at a depth of ~250 μm from the pia injected over 2–4 min and each injection site was separated by ~500 μm. Pipettes were left in the brain for 3 min after injection to avoid backflow. After virus injections, a chronic imaging window was implanted consisting of a glass plug glued onto a larger glass base. The edges between the glass plug and the skull were filled with 1.5% agarose and the window was secured using dental acrylic. Buprenorphine (0.1 mg kg^{-1}) was injected subcutaneously at the end of surgery.

Behaviour. Three days after surgery, mice were water-restricted at 1 ml per day. After ~14 days of water restriction, mice were trained daily for 14 days while two-photon imaging was applied simultaneously. The lever was built using a piezoelectric flexible force transducer (LCL-113G, Omega Engineering) attached to a 1/16-mm-thick brass rod. The voltage from the force transducer, which is proportional to the lever position, was continuously recorded using a data acquisition device (LabJack) and software (Ephus, MATLAB, Mathworks) working with custom software running on LabVIEW (National Instruments) which monitored threshold crossing. The behavioural setup was controlled by software (Dispatcher, Z. Mainen and C. Brody) running on MATLAB communicating with a real-time system (RTLinux). A 6-kHz tone marked a period during which lever-press was rewarded with water (~8 μl per trial) paired with a 500-ms, 12-kHz tone, followed by an intertrial interval (variable duration, see below). Lever-press was defined as crossing of two thresholds (~1.5 mm and ~3 mm below the resting position) within 200 ms. The 3-mm threshold defined the displacement required, and the 1.5-mm threshold ensured that the mouse did not hold the lever near the lower threshold. Failure to press during the cue period triggered a loud white noise and an intertrial interval. Lever presses during intertrial intervals were neither rewarded nor punished. The cue period was decreased during the first two sessions from 30 s to 10 s. The reward period was reduced during the first three sessions from 2 s to 0.4 s. The intertrial interval was increased over the first three sessions from 2–4 s to 8–12 s. Each session lasted 20–30 min and 100–200 trials until terminated when mice stopped performing or consumed 1 ml of water. Experiments lasted for 11–14 sessions. One mouse failed to learn the task and was thus excluded from all analyses.

Lesion. Motor cortex lesions were performed under isoflurane anaesthesia. After craniotomy was performed as above, cortical tissue was aspirated using a glass Pasteur pipette connected to vacuum. Care was taken to avoid damaging the underlying white matter. After the lesion, the cavity was filled with Surgifoam (Johnson & Johnson), KWIK-CAST (World Precision Instruments) and then with a layer of dental acrylic. Mice were allowed to recover for 3 days after the surgery and then placed on water restriction. Behavioural training started 2 weeks after lesion. The extent of lesion was determined for each mouse with post hoc histology.

Muscimol inactivation. Mice with imaging windows were first trained with the task for 7–14 days. On the day of inactivation, the imaging window was removed and ~70 nl of muscimol (5 μg/l μl in cortex buffer) was injected over 2–3 min in the centre of the craniotomy at the depth of 300 μm, under isoflurane anaesthesia. The craniotomy was then sealed and mice were allowed to recover in their home cage on a heating pad for 60 min before behavioural experiments. For control injections, muscimol was injected into the barrel cortex, using the coordinate of 1.4 mm posterior and 3.1 mm lateral from bregma.

Optogenetic inactivation. Surgery was performed on PV-Cre mice as above to inject AAV2/1-CAG-Flex-ChR2-tdTomato around the forelimb area of the motor cortex at five sites. 80 nl was injected at each site at each depth of 400 μm and 800 μm. Behavioural training started 3 weeks after surgery. After seven sessions of daily training, the cortical area was inactivated in 20% of trials by activating PV neurons[37] by blue light from an LED (~40 mW, 470 nm, Doric Lenses) delivered directly onto the centre of the craniotomy covered with a chronic glass window. Blue light was delivered starting from 1–2 s before the cue period until the end of the cue period (that is, reward delivery or time out). Blue light delivery was performed in seven successive sessions. In the last two sessions, the glass window was covered with curable silicone (KWIK-CAST, World Precision Instruments) and these served as control sessions.

Optogenetic microstimulation. Surgery was performed on C57BL/6 wild-type mice as above to inject AAV2/1-CAG-ChR2-Venus around the forelimb area of the motor cortex at 9 sites. 20 nl was injected at each site at the depth of 300 μm. Three weeks after surgery, mice were head-fixed. Blue light from an LED (~40 mW, 470 nm, Doric Lenses) was delivered directly onto the centre of the craniotomy covered with a chronic glass window for 1 s per trial with the intertrial interval of 8–12 s. Stimulation was performed without anaesthesia. The effect of the light stimulus on forelimb movements was quantified by manually identifying movie frames in which the forelimb movements were observed on videos cropped so that the optical stimulation was not visible. Pre-light periods were defined as movie frames lasting from 2 to 1 s before light onset. Scoring was done by two individuals independently and trials which differed between the scorers were excluded (1/79 light trials, 3/79 pre-light trials).

Imaging. Imaging was conducted with a commercial two-photon microscope (B-scope, Thorlabs) running Scanimage using a 16× objective (NIKON) with excitation at 925 nm (Ti-Sa laser, Newport). Imaging was always conducted in awake animals. For calcium imaging, images (512 × 512 pixels covering 472 × 508 μm) were recorded at approximately 28 Hz in continuous segments about 2 min long each with inter-segment intervals of 12 s. The trials that overlapped with the intervals were discarded. Signals for the start of each trial were also recorded, which were used to align images and behaviour data. Slow drifts in imaging field were manually corrected using reference images. For structural imaging, stacks of image planes (512 × 512 pixels covering 94 × 104 μm) were acquired at approximately 28 Hz, 20 frames per plane, 80–120 planes per animal with a z-axis step size of 1.0 μm between planes.

Movement analysis. Movement bouts were identified in the lever displacement traces (voltage recordings from the force transducer) that were down-sampled from 10 kHz to 1 kHz and then filtered (4-pole 10 Hz low-pass Butterworth). The velocity of the lever was then determined by smoothing the difference of consecutive points with a moving average window of 5 ms. The envelope of the velocity was then extracted using a Hilbert transform, and movement bouts were defined by the envelope crossing a threshold (4.9 mm per second). Each movement bout was extended by 75 ms, bouts separated by less than 500 ms were considered continuous, and then the start and end times were fine-tuned as follows. The start time was defined by finding when the lever position crossed a threshold exceeding the resting period before the movement, and the end time was defined by finding when the lever position went below a threshold defined by the resting period following the movement. Thresholds were the resting position plus the 99th percentile of noise distribution defined as the difference between the Butterworth smoothed trace and the original trace. These processes were chosen empirically based on visual inspection. For trial-based analyses, the trials in which animals were moving the lever at the onset of cue were excluded.

Image analysis. For calcium imaging data, lateral motion was corrected using full-frame cross-correlation image alignment (Turboreg[38] plugin for ImageJ). Motion within each frame was negligible due to the fast frame rate. Regions of interest (ROIs) were manually drawn using a custom MATLAB program by visually inspecting movies from all sessions and selecting neurons that showed at least one fluorescence transient in at least one session. Therefore, our analysis excludes neurons that do not show any fluorescence transients during our imaging periods. ROIs were aligned across sessions using a semi-automated method and classified as excitatory or inhibitory based on tdTomato expression. ROIs which presented with a nucleus filled by GCaMP5G at any point during the experiment, indicating possibly abnormal physiology[39], were excluded from all analyses. Other than these nucleus-filled neurons, GCaMP-expressing neurons have been shown to display normal physiological properties including input resistance, resting membrane potential, input–output relationship, synaptic input maps, and normal synaptic plasticity[8,39].

For structural imaging data, lateral motion for each image plane (20 frames) was corrected using full-frame cross-correlation image alignment (Turboreg[38] plugin for ImageJ), with the average of the five most consistent consecutive frames as the reference image. After this alignment, all 20 frames within a plane were averaged. Different image planes were then aligned using recursive alignment of stacks of images (Stackreg, plugin for ImageJ).

©2014 Macmillan Publishers Limited. All rights reserved

Fluorescence analysis. Pixels within each ROI were averaged to create a fluorescence time series. Background fluorescence fluctuations were subtracted from each ROI to remove neuropil contamination as follows. A ring-shaped 'background ROI' was created from the border of each neuronal ROI to a width of 6 pixels. From this background ROI, pixels containing transients that did not contaminate the neuronal ROI were excluded. These excluded pixels were identified as those that contained time points at which pixel values exceeded the neuronal ROI by two times the standard deviation of the difference between each background ROI pixel time series and the neuronal ROI time series. The remaining pixels were averaged to create a background fluorescence trace, and the ΔF of the background fluorescence trace was subtracted from the neuronal ROI fluorescence trace to create the final background-subtracted fluorescence trace for each neuronal ROI.

The time-varying baseline (F_0) of a fluorescence trace was estimated by smoothing inactive portions of the trace using the iterative procedure detailed below.

Inactive portions of the trace were initially estimated as when the raw trace loess-smoothed with a 1-s window was below a threshold. These inactive portions were further shortened by 5 s on each end to exclude tails of active portions. The threshold for activity was estimated by first creating a preliminary F_0 approximation, which was a 1-min moving average of the original fluorescence trace. This preliminary F_0 was subtracted from the raw trace to yield a preliminary ΔF. The noise of the fluorescence was calculated as the standard deviation of the difference between the preliminary ΔF and the smoothed preliminary ΔF (loess, 1 s). An offset of the preliminary F_0 was then estimated as the mode of the smoothed preliminary ΔF. The threshold for detecting active portions was then set as preliminary F_0 + the offset + two times the fluorescence noise. The remaining inactive portions of the trace were then concatenated and subjected to a second round of activity extraction using the same procedure, but by defining inactive portions where values fell within ± two times the fluorescence noise.

Inactive portions were concatenated and smoothed (loess, 1 s). The resulting smoothed trace was then broken up according to their original time points and values were linearly interpolated across gaps (that is, active portions), resulting in an F_0 estimation that was independent of activity and slow drifts. This F_0 estimation was fine-tuned for an offset as follows. The F_0 was subtracted from the raw trace, yielding a new ΔF. The fluorescence noise was once again estimated by the standard deviation of the difference between ΔF and smoothed ΔF (loess, 1 s). The offset was then estimated by the mode of Gaussian fit of the distribution of values of inactive portions of the ΔF. Inactive portions were defined as when the ΔF values were within ± two times the noise values, and were shortened by 5 s on either end. This offset was added to the F_0 estimation, yielding the final F_0.

Activity analysis. Activity event traces were created from normalized background-subtracted fluorescence traces. For excitatory neurons, events were defined if the first derivative (velocity) of the smoothed fluorescence trace (loess, 1 s) crossed five times the standard deviation of the inactive velocity trace (inactive velocity trace was derived from periods when the fluorescence was within three times the standard deviation of the fluorescence trace). This velocity criterion detected sharp rises in the fluorescence trace. For these detected events, the start and end times were defined using the following iterative process. The peak time of the event was first roughly estimated as the time when the velocity drops below zero for the first time after it crossed the threshold as above. The peak time (that is, the end time of the event) was then defined as the time of the highest $\Delta F/F_0$ value within five frames before and after the initial estimate. We next defined the 'baseline' $\Delta F/F_0$ value for the event as the $\Delta F/F_0$ value at the first time point when velocity was above zero before the peak time. (This 'baseline' $\Delta F/F_0$ for each event is similar to the baseline of the fluorescence trace (zero) except in cases when the event occurs during a decay of another event; see the last event in Extended Data Fig. 4b for such an example.) The start time of the event was then defined as the last time point before the peak time when the $\Delta F/F_0$ value is within noise level from the 'baseline' $\Delta F/F_0$ ('noise' being three times the standard deviation of the difference between the raw $\Delta F/F_0$ trace and the loess-smoothed $\Delta F/F_0$ trace.) An activity event trace was then constructed which was zero except for frames with detected events, and each event was assigned an amplitude equal to the difference between the peak $\Delta F/F_0$ and the 'baseline' $\Delta F/F_0$ for that event. This eliminated the decay of the calcium signal[19], but the use of velocity preserved events which occurred on top of the decays from other events. For inhibitory neurons, activity event traces were generated with the following procedure. The fluorescence noise was defined as the mean of the absolute difference between the raw trace and a 1 s moving window loess smoothed fluorescence trace. A low threshold of 1 times the noise and a high threshold of 3 times the noise were then set. Events were required to cross the high threshold. The start of an event was defined as the time when the fluorescence trace crossed the low threshold going up to capture the start of activity, and the end was defined as the time when the fluorescence trace crossed the high threshold going down. An activity event trace was then constructed which was zero at all frames except during detected events which were assigned values of the original $\Delta F/F_0$ for those frames.

Classification of movement-related neurons. We observed higher levels of activity during movement periods. In individual neurons, the average percentages of image frames that contained activity during movement periods versus non-movement periods were 0.68 ± 0.03% versus 0.23 ± 0.02% in excitatory neurons and 14.45 ± 0.49% versus 6.95 ± 0.27% in inhibitory neurons (mean ± s.e.m.). Neurons whose activity was significantly higher during movement periods were classified as movement-related using the following procedure. The amount of activity during movement was calculated for each neuron as the mean value of the activity event trace during movement epochs (defined as described above, and extending individual epochs by 5 image frames before and after each movement). The movement trace was then shuffled (10,000 times) such that complete movement epochs were kept intact but their position in the trace and relation to each other was randomized. A measure of activity during these shuffled movement epochs was calculated in each shuffle as above. The neuron was classified as movement-related if the real value was higher than the 0.5 percentile value of the shuffled values. Classification using only rewarded movements instead of all detected movements gave nearly identical results.

For analysing the longitudinal dynamics of the fractions of movement-related neurons over sessions (Fig. 2b), the fraction of movement-related neurons in each session in each animal was normalized to the highest and lowest values of the animal. The correlation was significantly positive for the data points in sessions 1–3 ($r = 0.60$, $P < 0.01$) and significantly negative for sessions 4–14 ($r = -0.36$, $P < 0.01$).

Population activity correlation. The stability of the population across days was assessed by correlation of population vectors (Fig. 2d). Each square represents the correlation coefficient of the excitatory neuron population activity vectors in a pair of sessions. The population activity vectors are the concatenation of the fraction of rewarded movements during which each neuron exhibited activity events. (For example, if neurons a, b and c are active in 20%, 70% and 30% of rewarded movements, respectively, then the population activity vector of the session is (0.2, 0.7, 0.3)).

Activity onset timing analysis. We performed two analyses to define the timing of activity of movement-related excitatory neurons relative to movement onset. To define when the population activity diverged from baseline, the activity of each neuron was first averaged across movements. Then the population activity vector in each image frame was compared to the baseline activity (all non-movement periods from all sessions) by bootstrap (10,000 repetitions), yielding a P value for each image frame. We identified image frames in which P values were below 0.01 in at least five successive frames, and defined the first frame of those as the time of divergence. The time of first population activity divergence from baseline was 105 ms before movement onset (Extended Data Fig. 6d). Similarly, to identify the timing of activity modulation of individual neurons, the activity of a neuron in each image frame across movements was compared to its baseline activity (420–315 ms before movement onset) by bootstrap (10,000 repetitions). We defined the activity onset timing as the first image frame in which P values were below 0.01 in at least five successive frames. 9.2% of movement-related excitatory neurons showed significant activity before movement onset (Extended Data Fig. 6f).

Analysis of movement–activity correlation. The relationship between movements and activity (Fig. 3) was analysed using 3 s (or 500 ms, Extended Data Fig. 7) starting from the onset of each rewarded movement, which was approximately the duration of rewarded movements for all animals over all sessions (2.62 ± 0.02 s, mean ± s.e.m.). The learned movement and activity patterns were created by averaging the lever traces and the activity of excitatory neurons, respectively, of a randomly chosen half of the trials of sessions 10–14, considered the expert stage. The trials used to generate the learned patterns were excluded from correlation analysis. The movement correlation for each trial was the correlation coefficient of the lever trace of the rewarded movement in that trial with the learned movement pattern. The activity correlation for each trial was the correlation coefficient between the concatenated activity time series of all excitatory neurons in the trial and the concatenated learned activity pattern. For results shown in Fig. 3b, the random choice of trials to define the learned patterns was repeated 1,000 times and the results were averaged.

Dendritic spine dynamics. Dendritic spines were manually scored over the entire 14 training sessions using a custom-written IGOR program (J. Boyd and K. Haas). Spine analysis was done in three dimensions and the criteria were as previous described[31]. Analysis was done blind to the session number of each image, which was randomized. We assumed that rapid 'flickering' of spines (elimination and immediate reformation, or formation and immediate elimination) is rare and corrected our blind scoring accordingly. While this corrected for mistakes in scoring, we may be slightly underestimating spine dynamics. Specifically, if a spine was scored as absent in one session (session X) and present in the immediately preceding (session X−1) and following (session X+1) sessions, then it was called present on session X. Furthermore, if a spine was scored as present in one session (session X) and absent in the immediately preceding (session X−1) and following (session X+1) sessions, then it was called absent on session X. No more than one correction was applied on any given spine. If a spine score contained these gaps after one correction, that spine was excluded from following analyses. These exclusions were rare (4 of 191). 8% of spines were

©2014 Macmillan Publishers Limited. All rights reserved

corrected (16 of 191). The results closely matched those from independent scoring of the same data without shuffling dates (data not shown).

Simultaneous two-photon guided cell-attached recordings and calcium imaging. Mice that had previously been used for calcium imaging were allowed full access to water before electrophysiology. On the day of the experiment, mice were anaesthetized with isoflurane and the glass window was removed and replaced with a glass half-window which was secured with superglue. The animals were then head-fixed in the imaging rig and allowed to recover from anaesthesia. Loose patch recordings were performed with glass pipettes (~5–7 MΩ) filled with 100 μM Alexa Fluor 488 in saline. Excitatory neurons (negative for tdTomato) expressing GCaMP5G without fluorescence in the nucleus were targeted for recording. Signals were amplified 500× by an Axon CNS amplifier (Molecular Devices), filtered at 2 kHz, recorded (Ephus) at 10 kHz, and synchronized to the start of image acquisition. In 4 out of 6 neurons, imaging was done at the same zoom as the population imaging experiments (field of view 472 × 508 μm), and at three times higher zoom for the other two neurons. The results were similar at both zooms.

Statistics. Non-parametric tests were used when possible to avoid assumptions about data distributions. Sample sizes were determined based on the statistical significance of our main findings, which is highly significant. Multiple comparisons were corrected for by Bonferroni corrections. Sample sizes (n) are as follows where applicable. Mice per session: 6, 6, 7, 7, 7, 7, 7, 7, 7, 7, 7, 6, 6, 5. Imaged, rewarded trials without movement at cue/total trials per session: 98/313, 173/526, 458/968, 488/1,071, 438/966, 519/1,081, 424/946, 453/1,082, 320/784, 457/981, 481/889, 417/959, 412/853, 280/702. Movement-related/all imaged excitatory neurons: 79/874, 118/874, 202/1,122, 210/1,122, 201/1,122, 213/1,122, 181/1,122, 191/1,122, 159/1,122, 171/1,122, 158/1,122, 136/995, 149/995, 89/843. Movement-related/all imaged inhibitory neurons: 103/262, 117/262, 155/297, 167/297, 154/297, 133/297, 133/297, 124/297, 106/297, 125/297, 119/297, 119/260, 114/260, 68/183.

31. Holtmaat, A. *et al.* Long-term, high-resolution imaging in the mouse neocortex through a chronic cranial window. *Nature Protocols* **4,** 1128–1144 (2009).
32. Li, C. X. & Waters, R. S. Organization of the mouse motor cortex studied by retrograde tracing and intracortical microstimulation (ICMS) mapping. *Can. J. Neurol. Sci.* **18,** 28–38 (1991).
33. Pronichev, I. V. & Lenkov, D. N. Functional mapping of the motor cortex of the white mouse by a microstimulation method. *Neurosci. Behav. Physiol.* **28,** 80–85 (1998).
34. Ferezou, I. *et al.* Spatiotemporal dynamics of cortical sensorimotor integration in behaving mice. *Neuron* **56,** 907–923 (2007).
35. Ayling, O. G., Harrison, T. C., Boyd, J. D., Goroshkov, A. & Murphy, T. H. Automated light-based mapping of motor cortex by photoactivation of channelrhodopsin-2 transgenic mice. *Nature Methods* **6,** 219–224 (2009).
36. Tennant, K. A. *et al.* The organization of the forelimb representation of the C57BL/6 mouse motor cortex as defined by intracortical microstimulation and cytoarchitecture. *Cereb. Cortex* **21,** 865–876 (2011).
37. Olsen, S. R., Bortone, D. S., Adesnik, H. & Scanziani, M. Gain control by layer six in cortical circuits of vision. *Nature* **483,** 47–52 (2012).
38. Thevenaz, P., Ruttimann, U. E. & Unser, M. A pyramid approach to subpixel registration based on intensity. *IEEE Trans. Image Process.* **7,** 27–41 (1998).
39. Tian, L. *et al.* Imaging neural activity in worms, flies and mice with improved GCaMP calcium indicators. *Nature Methods* **6,** 875–881 (2009).

©2014 **Macmillan Publishers Limited. All rights reserved**

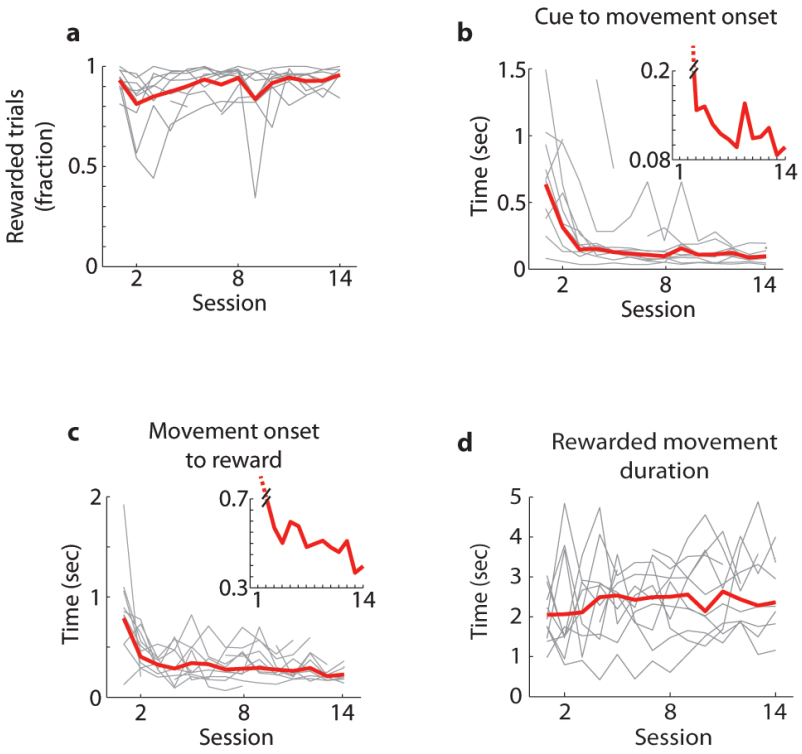

Extended Data Figure 1 | Behaviour. The fraction of rewarded trials is consistently high but the timing of behaviour improves during learning. **a**, Fraction of trials that are rewarded. **b**, Time from cue onset to movement onset decreases ($P < 0.001$, one-way ANOVA); inset, zoom. **c**, Time from movement onset to reward decreases ($P < 0.001$, one-way ANOVA); inset, zoom. **d**, The duration of each rewarded movement is stable throughout learning ($P = 0.94$, one-way ANOVA). Grey, individual mice; red, mean of all animals (**a**) or median of all trials (**b**–**d**).

©2014 Macmillan Publishers Limited. All rights reserved

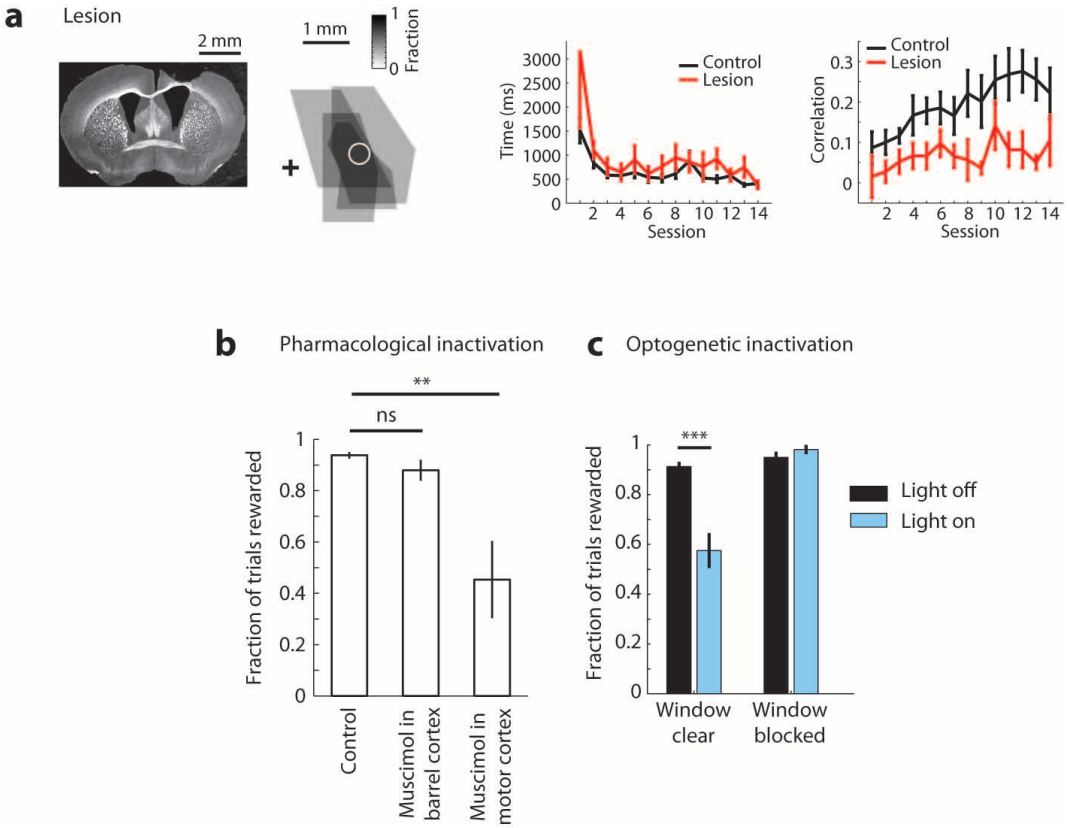

Extended Data Figure 2 | Motor cortex is required for the lever-press task. **a**, Aspiration lesion of motor cortex impairs learning. Mice were allowed to recover for 14 days after lesion before training. Left: histological image showing lesion in the right motor cortex and quantification of lesion extents in four mice shown as a density map of the fraction of animals in which the area was lesioned. Anterior is to the top; lateral to the right. + denotes bregma. The white circle indicates the imaged area. Middle: average time from movement onset to reward throughout learning. This time is longer in mice with motor cortex lesion ($P < 0.01$, two-way ANOVA), indicating that the mice with a lesion are less efficient in their movements. Right: correlation of lever movements in all pairs of trials within each session throughout learning. This correlation is lower in the mice with a lesion ($P < 0.001$, two-way ANOVA), indicating that the mice with a lesion do not develop reproducible movements. **b**, Injections of muscimol, a GABA receptor agonist, into the imaged area acutely impairs performance (control versus muscimol in motor cortex, $^{**}P < 0.01$, Wilcoxon rank sum test). Muscimol injections in the barrel cortex had no significant effect (control versus muscimol in barrel cortex, $P = 0.35$, Wilcoxon rank sum test). Control, $n = 18$ sessions in 6 mice; barrel cortex, $n = 6$ sessions in 6 mice; motor cortex, $n = 6$ sessions in 6 mice. **c**, The imaged cortical area was acutely inactivated by stimulation of ChR2 in parvalbumin-expressing inhibitory neurons by blue light in interleaved 20% of trials ($n = 10$ sessions in 2 animals). This optogenetic inactivation of the imaged area impaired performance on a trial-by-trial basis ($^{***}P < 0.001$, Wilcoxon rank sum test). Blue light had no effect on behaviour when the window was covered with opaque silicone ($n = 4$ sessions in 2 animals). All error bars are s.e.m.

©2014 Macmillan Publishers Limited. All rights reserved

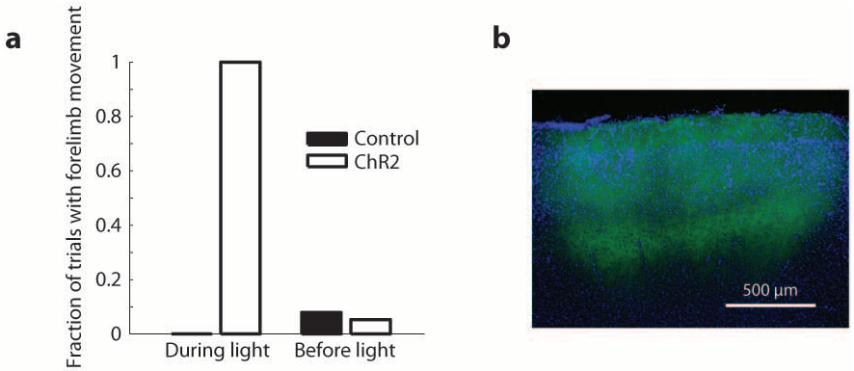

Extended Data Figure 3 | Optogenetic stimulation of the imaged area evokes forelimb movements in awake mice. **a**, Optogenetic excitation of the imaged area triggers forelimb movements in mice expressing ChR2 but not in control mice not expressing ChR2 ($P < 0.001$, chi-squared test). ChR2 expression does not alter spontaneous movement frequency in the absence of stimulation ($P = 0.64$, chi-squared test). 'During light', 1-s light stimulation; 'before light', 2 to 1 s before light onset, $n = 40$ 'during light' trials and 38 'before light' trials in two ChR2 mice, 38 'during light' trials and 38 'before light' trials in two control mice. **b**, Histological section showing the expression of ChR2 in the motor cortex. Green, ChR2–YFP; blue, DAPI.

©2014 Macmillan Publishers Limited. All rights reserved

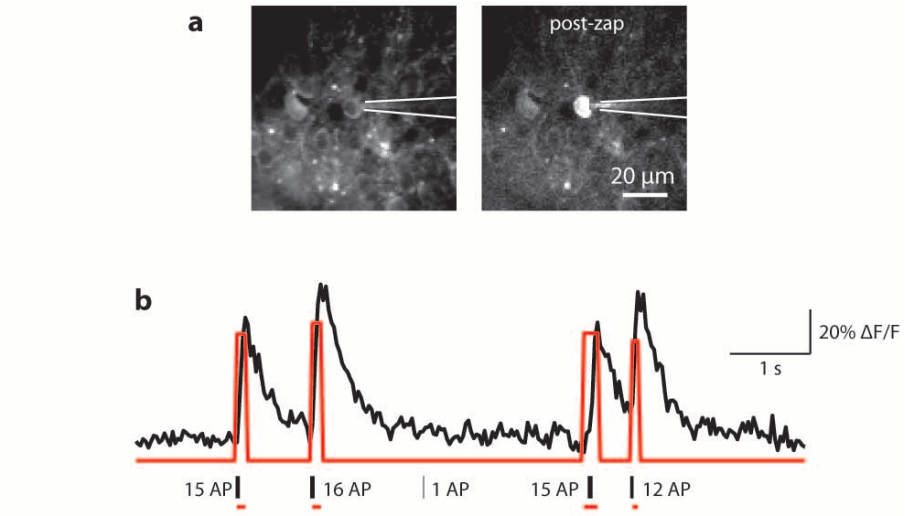

c

Neuron	1	2	3	4	5	6	Combined
Median offset (ms)	19.0	10	21.8	17.2	-39.1	-8.5	7.1
SD (ms)	62.9	17.4	44.5	30.9	48.9	34.8	41.4
# of events	12	16	17	24	9	30	108

Extended Data Figure 4 | Simultaneous cell-attached recordings and two-photon calcium imaging in awake mice. **a**, Left: *in vivo* two-photon image of motor cortex neurons expressing GCaMP5G. The neuron in the centre is targeted with a patch electrode. Right: after the recording session, voltage step was applied to the electrode to activate the recorded neuron. The increased GCaMP5G fluorescence in the middle neuron confirms that the neuron was indeed targeted. **b**, Example GCaMP5G fluorescence trace (top: black indicates fluorescence trace and red indicates detected calcium events) and simultaneously recorded action potentials (bottom: black vertical ticks; the numbers indicate the number of action potentials contained in each burst). Horizontal red lines at bottom indicate the duration of detected calcium events. Note the precise temporal relationship between action potentials and calcium events. **c**, Table summarizing data from six neurons in two mice. Positive offsets indicate the lag of the onset of detected calcium events relative to the first spike in the burst. The offset (7.1 ± 41.4 ms) is on the order of the temporal resolution of our imaging (~35 ms per image frame).

©2014 Macmillan Publishers Limited. All rights reserved

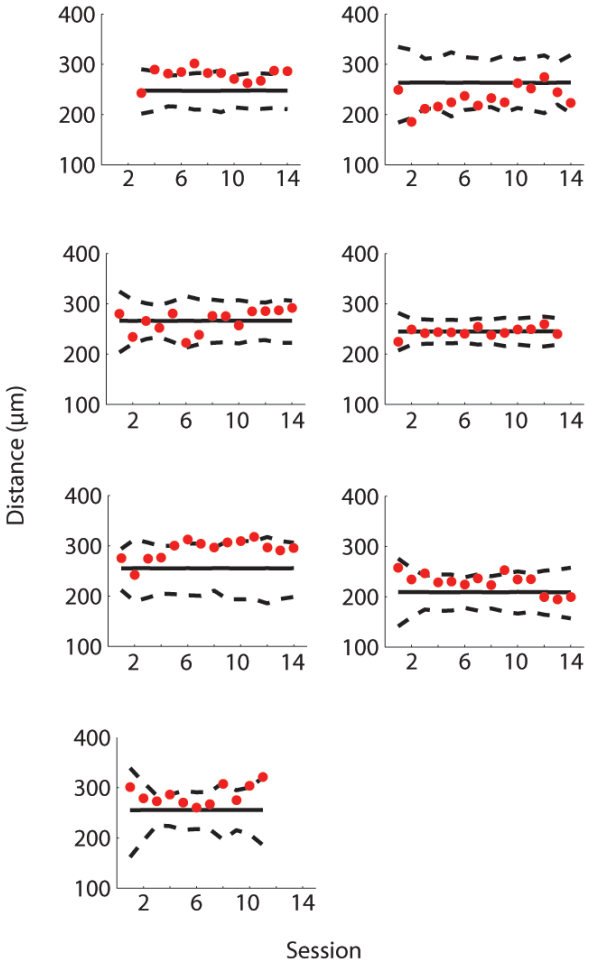

Extended Data Figure 5 | Lack of spatial clustering of movement-related excitatory neurons. Each plot represents one animal. Red dots show the mean pairwise distance between movement-related excitatory neurons. Solid and dotted black lines show the mean and 95% confidence intervals, respectively, obtained from shuffling the identities of movement-related neurons among all excitatory neurons 10,000 times. Dots below the lower dotted line would indicate significant clustering of cells, whereas dots above the upper dotted line would indicate the significant dispersion of cells ($P < 0.05$).

©2014 Macmillan Publishers Limited. All rights reserved

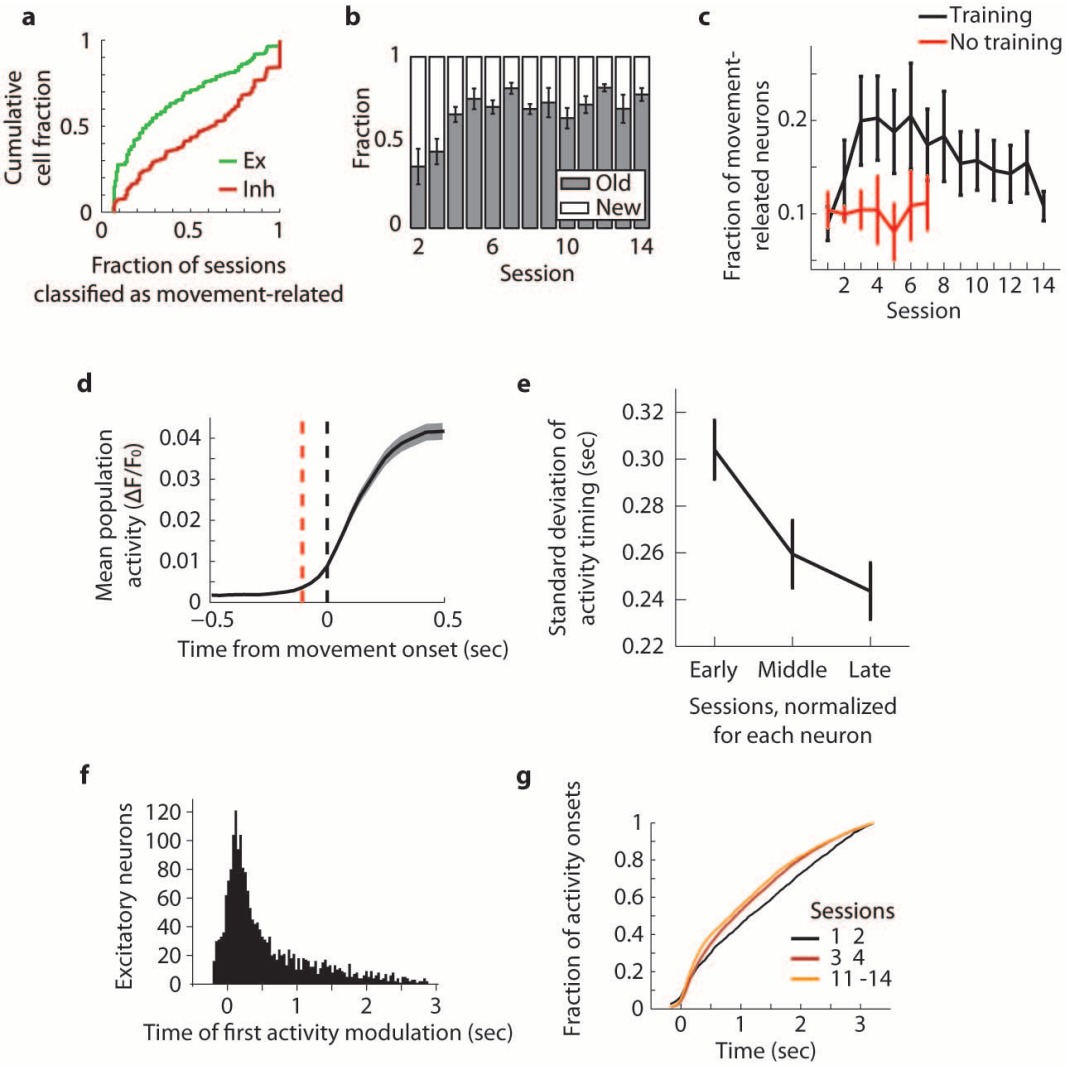

Extended Data Figure 6 | Additional analysis of population activity. **a**, Cumulative distribution of fraction of sessions classified as movement-related for inhibitory (red) and excitatory (green) neurons, showing the relative invariance of inhibitory neurons and dynamism of excitatory neurons ($P < 0.001$, Kolmogorov–Smirnov test). **b**, Movement-related excitatory neuron populations in each session compared to the previous session. Grey, fraction of neurons classified in the previous session; white, not classified in the previous session. A large number of newly movement-related neurons were added in the first few sessions ($P < 0.001$, comparison between sessions 2–4 versus 10–14, Wilcoxon rank sum test). **c**, Fraction of excitatory neurons classified as movement-related in each session. Black, training ($n = 7$ mice, this is the data shown in Fig. 2b); red, no training ($n = 6$ mice). The expansion of movement-related neurons is specific to animals that underwent training ($P = 0.74$, sessions 1–2 combined; $P < 0.001$, sessions 3–7 combined; Wilcoxon rank sum test). **d**, Average population activity aligned to movement onset (black dotted line). Average activity (calcium event trace) of each movement-related excitatory neuron was averaged. The population activity diverged from baseline 105 ms before movement onset (red dotted line, Methods). **e**, Standard deviation of activity timing of individual movement-related excitatory neurons across sessions. Focusing on neurons that are classified as movement-related in three or more sessions, the standard deviation of activity onset timing relative to movement onset is plotted across sessions. Sessions were binned into one-third of the total number of sessions each neuron was classified. Activity timing became more stable on the neuron-by-neuron basis ($r = -0.14$, $P < 0.001$). **f**, Histogram of the time from movement onset that the activity of each movement-related neuron significantly diverged from baseline. 9.2% of movement-related excitatory neurons show significant pre-movement activity, a composition similar to a previous study[14]. 82.7% of activity of movement-related neurons occurred during the periods between 105 ms before movement onset and movement offset (Methods). **g**, The cumulative fraction plot of the timing of all activity onsets of movement-related excitatory neurons during rewarded movements. Each group of sessions is shown as a line, with different colours representing different sessions. The distribution of activity onset timing during later sessions shifts towards the movement onset ($P < 0.001$, Kolmogorov–Smirnov test for all three comparisons). All error bars are s.e.m.

©2014 Macmillan Publishers Limited. All rights reserved

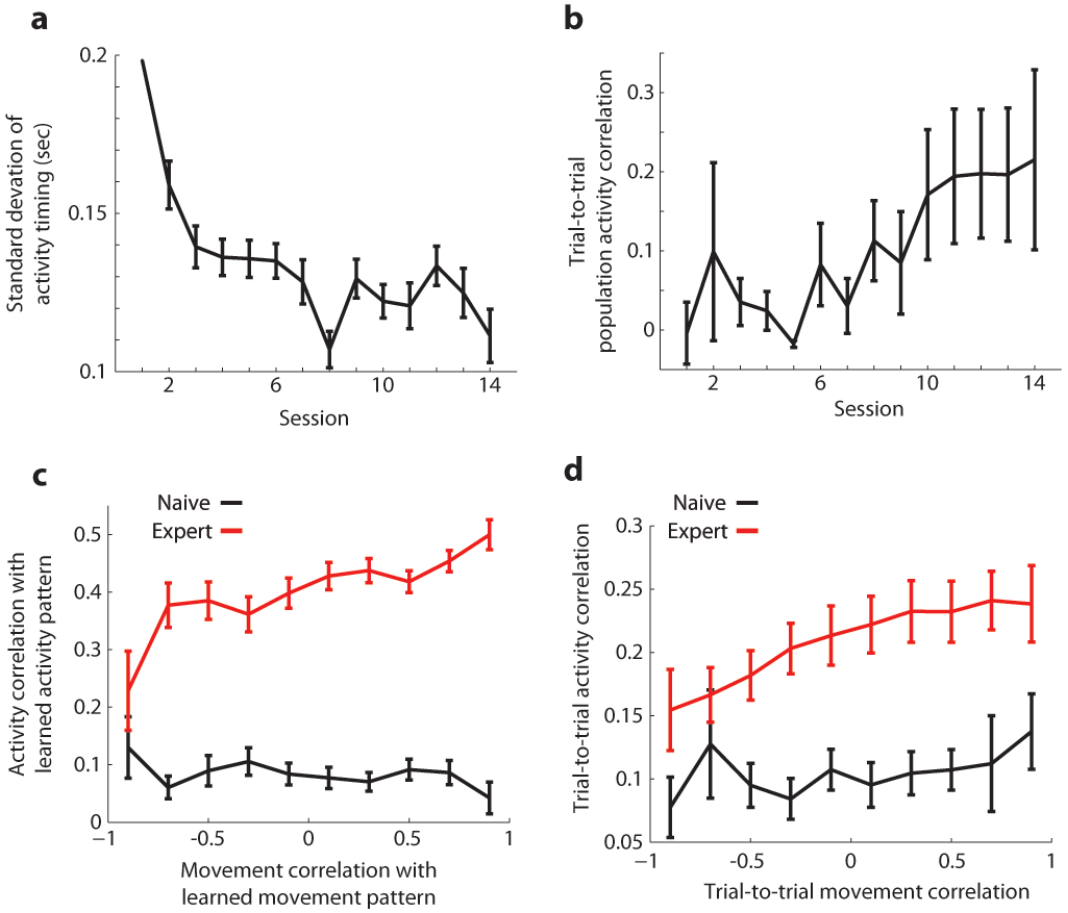

Extended Data Figure 7 | Activity analysis focusing on the first 500 ms of each movement. For the activity analyses in the main figures that used the duration of 3 s after movement onset, we repeated the same analyses focusing on the first 500 ms of each movement (median time from movement onset to reward = 506 ms). This early activity shows progression throughout learning, similar to when activity over 3 s was considered. **a**, Standard deviation of the timing of activity onsets for movement-related excitatory neurons over sessions, indicating a gradual refinement of activity timing ($r = -0.18$, $P < 0.001$). Neurons that were active in less than five trials of a given session were excluded from this analysis. The first bin contains only one data point and thus does not have an error bar. This analysis is equivalent to Fig. 2g. **b**, Pairwise trial-to-trial correlation of temporal population activity vectors increases with learning ($r = 0.38$, $P < 0.001$). Temporal population activity vector was defined as a concatenation of the activity traces of all movement-related neurons and thus maintained temporal information within each movement. This analysis is equivalent to Fig. 2h. **c**, Correlation of spatiotemporal activity with the learned activity pattern is a function of the correlation of movement with the learned movement pattern in expert sessions. Movements similar to the learned movement pattern but made in naive sessions display activity very different from the learned activity pattern ($P = 0.28$ and <0.001 in the bins 1 and 2–10, respectively, Wilcoxon rank sum test). This analysis is equivalent to Fig. 3b. **d**, Pairwise trial-to-trial correlation of temporal population activity vectors plotted as a function of movement correlation on those trials. A strong relationship between population activity and movement emerges during learning ($P = 0.08$, $= 0.08$, $= 0.004$, <0.001, $= 0.002$, <0.001, $= 0.001$, $= 0.002$, <0.001 and $= 0.046$ for each bin, Wilcoxon rank sum test). This analysis is equivalent to Fig. 3c. All error bars are s.e.m.

©2014 Macmillan Publishers Limited. All rights reserved

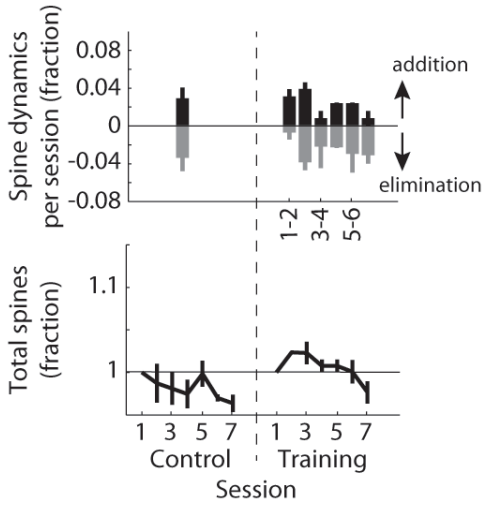

Extended Data Figure 8 | Dynamics of dendritic spines in the hindlimb area during learning of the lever-press task. Summary of dendritic spine dynamics in the hindlimb area during control period (7 days before training) and subsequent 7 days of training. Mice were water restricted in both conditions. Top: spine additions (black) and eliminations (grey) in each session. For control sessions, data from all sessions are combined. Bottom: total spine number across sessions. Values are normalized to the total spine number in session 1 in each condition. Unlike the forelimb area, the density of dendritic spines in the hindlimb area is relatively stable during learning ($P = 0.07$, comparisons between control versus training sessions 4–7, Wilcoxon rank sum test). All error bars are s.e.m.

©2014 Macmillan Publishers Limited. All rights reserved

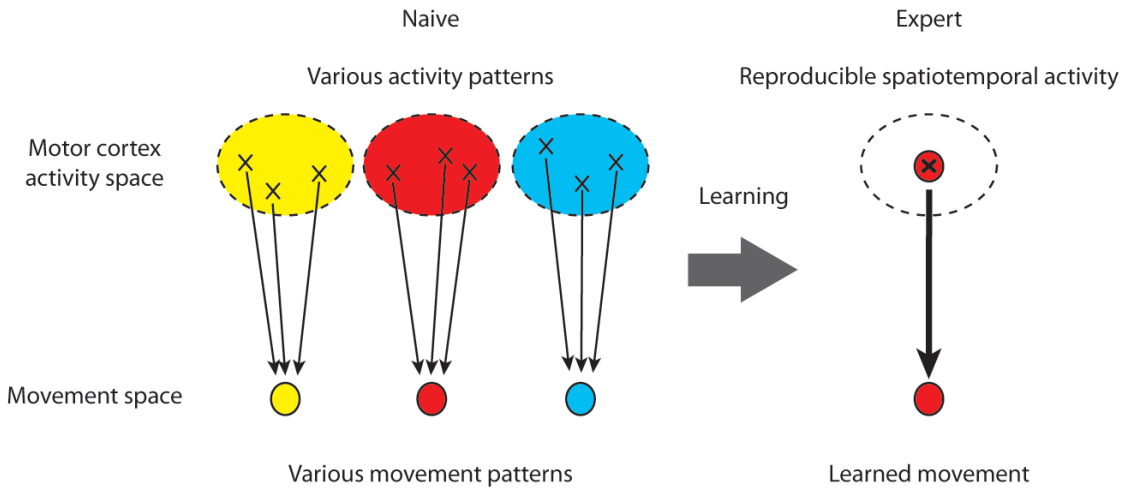

Extended Data Figure 9 | Schematic of learning-related changes in the relationship of motor cortex activity and movement. Top: abstract space of activity patterns. Bottom: abstract space of movements. Circles in the movement space represent observed movements, and ovals in the activity space represent possible activity patterns that can lead to corresponding movements. Crosses and arrows represent example individual trials of activity–movement pairs. In naive animals, each trial involves variable activity and movement patterns as illustrated by scattered crosses and multiple movements. In this stage, the relationship between activity and movement is inconsistent (that is, degenerate), such that same movement is derived from different activity patterns in different trials. During learning, this degeneracy is reduced and a reproducible spatiotemporal activity pattern emerges in the motor cortex that reliably generates the learned movement. This learned activity pattern (bold cross) is rarely, if at all, observed in naive stages.

©2014 Macmillan Publishers Limited. All rights reserved